Nanoscale

PAPER

View Article Online
View Journal | View Issue

Check for updates

Cite this: *Nanoscale*, 2018, **10**, 2936

Band gap modification and photoluminescence enhancement of graphene nanoribbon filled single-walled carbon nanotubes†

A. I. Chernov, *[a] P. V. Fedotov,[a] H. E. Lim,‡[b] Y. Miyata,[c] Z. Liu,[d,e] K. Sato,[d] K. Suenaga,[d] H. Shinohara[b] and E. D. Obraztsova[a]

Molecule encapsulation inside the single-walled carbon nanotube (SWCNT) core has been demonstrated to be a successful route for the modification of nanotube properties. SWCNT diameter-dependent filling results in band gap modification together with the enhancement of photoluminescence quantum yield. However, the interaction between the inner structure and the outer shell is complex. It depends on the orientation of the molecules inside, the geometry of the host nanotube and on several other mechanisms determining the resulting properties of the hybrid nanosystem. In this work we study the influence of encapsulated graphene nanoribbons on the optical properties of the host single-walled carbon nanotubes. The interplay of strain and dielectric screening caused by the internal environment of the nanotube affects its band gap. The photoluminescence of the filled nanotubes becomes enhanced when the graphene nanoribbons are polymerized inside the SWCNTs at low temperatures. We show a gradual photoluminescence quenching together with a selective signal enhancement for exact nanotube geometries, specifically (14,6) and (13,8) species. A precise adjustment of the optical properties and an enhancement of the photoluminescence quantum yield upon filling for nanotubes with specific diameters were assigned to optimal organization of the inner structures.

Received 21st September 2017,
Accepted 28th December 2017

DOI: 10.1039/c7nr07054c

rsc.li/nanoscale

Published on 29 December 2017. Downloaded by Boston College on 7/14/2018 1:14:02 PM.

Introduction

Carbon nanotubes provide a unique template for nanoscale engineering.[1] The inner space of nanotubes with diameters of 1–2 nm is enough to accommodate large dye molecules,[2–4] polycyclic aromatic hydrocarbon molecules[4–7] or various fullerenes[8–10] inside. Nanotube confinement allows performing chemical reactions inside[11] and also leads to structural transformation of encapsulated molecules.[12–15] Recently, the nanotube core was used as a nanoreactor for the formation of sp^1-hybridized carbon chains.[16] The stability and length of the linear carbon chain strongly depend on the nanotube diameter. Single-walled carbon nanotubes (SWCNTs) can be also used for the formation of sp^2-hybridized carbon materials – graphene nanoribbons (GNRs).[7,10] The nanotube diameter determines the arrangement of the filler molecules and the result of polymerization. In the case of coronene molecule encapsulation several types of inner structures can be created including coronene stacks,[17–19] molecule dimers[20] and, finally, GNRs. All types of hybrid nanomaterials demonstrate different optical properties.[19,21] One of the strategies to obtain the material with desired parameters is by the use of preliminarily separated SWCNTs with equal properties (in terms of geometry or conductivity type). Recent progress in separation techniques[22,23] has opened up a wide range of methods to control the nanotube diameter. The nanotubes with a chosen geometry can be used further for the filling and formation of hybrid nanomaterials with desired properties. However, it should be noted that the preparation procedures required for the separation techniques may significantly change the physical properties of SWCNTs,[24] consequently resulting in complicated phenomena in the filled hybrid materials.

Along with that, the encapsulated structures themselves can successfully modulate the nanotube properties. Charge-carrier doping can be used for fine-tuning the 1D electronic transport characteristics,[25,26] which is desirable for nanoelectronics.

[a]*Prokhorov General Physics Institute RAS, Moscow, 119991, Russia. E-mail: al.chernov@nsc.gpi.ru*
[b]*Department of Chemistry, Nagoya University, Nagoya 464-8602, Japan*
[c]*Department of Physics, Tokyo Metropolitan University, Hachioji 192-0397, Japan*
[d]*Nanomaterials Research Institute, National Institute of Advanced Industrial Science and Technology (AIST), Tsukuba 305-8565, Japan*
[e]*Inorganic Functional Materials Research Institute, National Institute of Advanced Industrial Science and Technology (AIST), Nagoya, Aichi, 463-8560, Japan*

†Electronic supplementary information (ESI) available. See DOI: 10.1039/c7nr07054c

‡Present address: Institute of Advanced Energy, Kyoto University, Uji 611-0011, Japan.

This journal is © The Royal Society of Chemistry 2018

Published on 29 December 2017. Downloaded by Boston College on 7/14/2018 1:14:02 PM.

Moreover, filling the nanotubes may influence the optical properties of SWCNTs.[27–29] A selective photoluminescence (PL) enhancement for some particular nanotube geometries has recently been reported.[27,30] The increase of the PL emission quantum yield of the hybrid material can be implemented in sensing applications, when SWCNTs serve as robust nanoemitters. Encapsulation of molecules and other nanostructures inside the nanotube channel can result in improved PL properties, reduced line widths and shifted peak positions of the excitonic optical transitions. However, the origin of the observed effects is complicated and may be an interplay between several factors. In the case of fullerene encapsulation that leads to the nanotube optical band gap variation,[31,32] the major contribution was assigned to the strain induced effects. While for the encapsulation of ferrocene molecules ($FeCp_2$) the PL properties modification was explained by the peculiar charge transfer[27] together with the molecular orientation depending on the host nanotube diameter.[33] The aforementioned processes can result in the increase of the PL quantum yield of SWCNTs. The enhancement effects occur not for all of the filled nanotubes, but for certain geometries. Understanding the processes taking place in the filled SWCNTs will make it possible to realize the controllable selective enhancement of PL quantum yield and to perform an accurate adjustment of hybrid material properties.

In this contribution, we use PL excitation to study in detail the behavior of several nanotube geometries after filling with coronene molecules, which were further converted into GNRs. We find that, depending on the GNR formation conditions, different SWCNT geometries demonstrate a PL enhancement. The PL intensity redistribution between the nanotube geometries is stepwise upon filling, with a trend for quenching of PL for the smallest diameter tubes and the existence of one dominant nanotube geometry, for which PL quantum yield is increased upon filling.

Both strain and dielectric screening affect the optical properties of the GNR@SWCNTs systems. We detect up to 1.7-fold PL enhancement for the nanotubes filled with low-temperature formed GNRs compared to pristine nanotubes.

Experimental

Synthesis of graphene nanoribbons inside single-walled carbon nanotubes

SWCNTs with an average diameter of 1.4–1.6 nm have been used in the study (Type SO, Meijo Nano Carbon). The nanotube filling was performed *via* a vapor phase encapsulation of coronene molecules (95%, TCI). The formation of low-temperature graphene nanoribbons inside SWCNTs was performed by loading into the separate compartments of an H-type pyrex tube 6 mg of open-capped SWCNTs and 10 mg of coronene powder, further degassing and sealing in an ampule (10^{-6} Torr). After heating at 450 °C for 48 h, the resulting carbon nanotubes were washed with 50 mL of toluene, dried and stored. The high temperature graphene nanoribbons inside SWCNTs were synthesized by additional heating of low-temperature-grown samples in a vacuum (10^{-6} Torr) at 700 °C for 48 h to induce further polymerization among the molecules encapsulated.[5,34]

Preparation of aqueous suspensions

2 mg of test samples (pristine SWCNTs, low temperature graphene nanoribbons inside SWCNTs and high temperature GNR@SWCNTs) were dispersed in 10 mL of D_2O with 1 wt% sodium cholate (SC, 98%, Kishida) for 20 h by using a bath type sonicator (Nanoruptor NR-350, Cosmo Bio). The dispersant was centrifuged at 52 000 rpm using a swing bucket rotor (S52ST, Hitachi) for 1 h to precipitate aggregated nanotube bundles. 80% of the supernatant was collected from the test tubes and used for optical measurements. The suspension fractions were diluted to common extinction at 1000 nm.

Optical investigation of materials

Absorption measurements were performed in a 10 mm path length quartz cuvette using a UV-vis-NIR double-lined spectrophotometer (PerkinElmer Lambda 950). The spectral resolution was 0.5 nm in the 200–3000 nm (6.2–0.41 eV) spectral range.

The photoluminescence spectra were recorded using a Horiba Jobin-Yvon "NanoLog-4" system supplied with an InGaAs IR enhanced range CCD detector (1100–2000 nm). A photoluminescence excitation in the vis–near-IR spectral range (740–1100 nm) was performed using a tunable cw Ti:Sapphire laser (Spectra-Physics Model 3900S pumped by Millennia Pro); an excitation in the UV-vis spectral range for the additional data was performed using a Xe lamp (250–900 nm). For the PL excitation maps the step between the excitation lines was 5 nm. In order to clearly observe and estimate the shifts in the PL data all the measurements (excitation and emission profiles) were fitted using previously reported procedures.[35]

Results and discussion

One type of molecule has been chosen for encapsulation inside SWCNTs. Coronene molecules ($C_{24}H_{12}$) demonstrate high filling rates and get easily polymerized inside the nanotube channel. In order to study the influence of the inner structures on the optical properties of SWCNTs we used two different sets of synthesis parameters. The first batch of samples was synthesized under low temperature polymerization conditions below 450 °C that resulted in the formation of short length graphene nanoribbons inside the nanotubes (LT GNR@SWCNTs) and the second set comprised samples formed at higher temperatures, reaching 700 °C. A high temperature polymerization resulted in the formation of fully ordered ribbons with a spiral organization (HT GNR@SWCNTs) along the whole nanotube length. A structure model of the studied HT GNR@SWCNT system is presented in Fig. 1(a). Raman spectroscopy measurements performed at

Published on 29 December 2017. Downloaded by Boston College on 7/14/2018 1:14:02 PM.

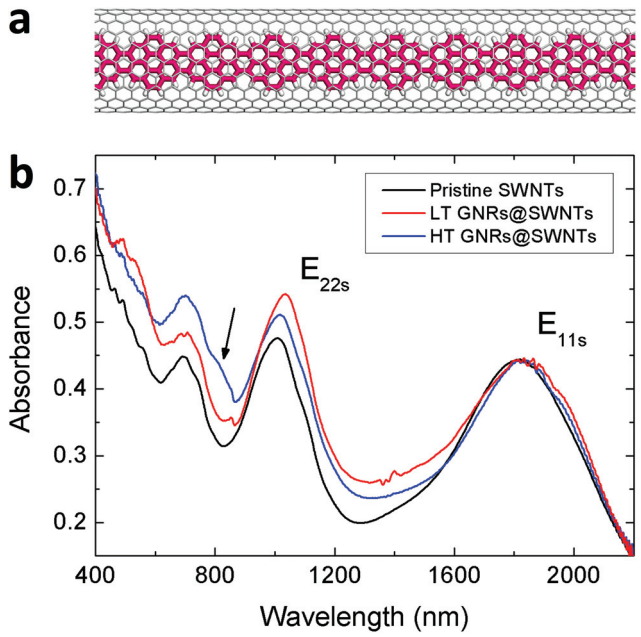

Fig. 1 (a) Structure model of an infinitely long GNR inside SWCNT. (b) Optical absorption spectra of pristine SWCNTs (black), low-temperature-grown GNRs@SWCNTs (red), and high-temperature-grown GNRs@SWCNTs (blue). Note the E_{22s} optical transition central peak position as it gets clearly shifted after the filling of nanotubes. The arrow marks the additional spectral feature from the high-temperature polymerized GNRs. Spectra are normalized to the E_{11s} transition.

two excitation energies are presented in the ESI (Fig. S1 and S2†). High resolution transmission electron microscopy (HR TEM) images of both types of samples can be found in ESI Fig. S3† and elsewhere.[5] It is important to note that high-resolution imaging even at low accelerating voltages is complicated for such composite materials as the hydrogen atoms get easily detached from the ribbon edges under irradiation.[36] Nevertheless, TEM images demonstrate the differences between the two sets of samples. The LT GNRs are seen as less organized within the nanotube channel, while the HT GNRs form long well-ordered structures. Both types of structures demonstrate the change in the host nanotube cross section due to the filling. All of the nanotubes used in the study have diameter distributions around 1.4–1.6 nm and can be filled by coronene molecules. The limit for the filling was previously estimated to be 1.1–1.2 nm.[17,19,21]

The differences between the two types of systems can be detected by optical absorption spectroscopy (Fig. 1b). In addition to the spectral features arising from the pristine mixture of semiconducting (s) and metallic (m) single-walled carbon nanotubes, such as the E_{11s} optical transition (1500–2100 nm), E_{22s} (800–1200 nm), E_{11m} (600–800 nm), and E_{33s} (400–600 nm) one can notice an extra band around 750 nm that is a signature of the HT GNRs (Fig. 1).[5] Peak positions of the absorption peaks get shifted after the nanotube filling. For instance, for both types of samples filled with LT and HT GNRs E_{11s} and E_{22s} band shifts can be clearly seen. Variation of the temperature during the polymerization influences the optical transitions of the filled nanotubes. The optical absorption measurements have been performed in an identical D_2O environment with the same amount of sodium cholate used as a surfactant.

In order to study the influence of filling on the nanotube band gap modification and to access the changes for each geometry of semiconducting nanotubes, we perform the photoluminescence excitation mapping (Fig. 2). Two main observations can be made from the PLE maps. First, the excitation and emission peak positions get changed for each geometry after the filling in comparison with the pristine nanotubes. Second, there is a PL intensity redistribution between the nanotube geometries for high- and low-temperature filling. While the brightest emitting nanotubes in the pristine sample are (11,9) and (14,6) species, for LT GNR filled tubes the dominant emission is shifted towards the (14,6) species and for high-temperature ones the brightest become (13,8) filled nano-

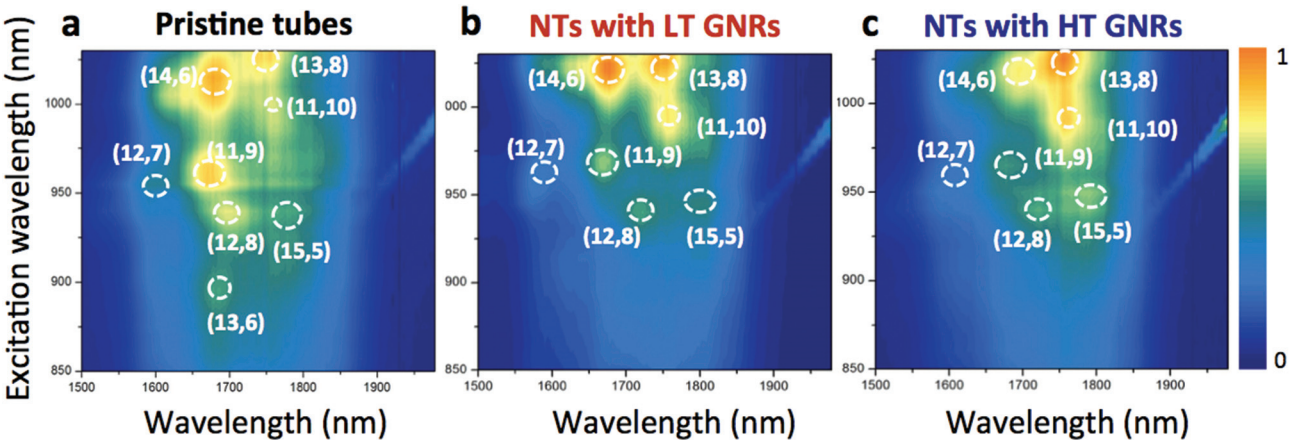

Fig. 2 Photoluminescence contour plots of pristine SWCNTs (a), low-temperature-grown GNRs@SWCNTs (b), and high-temperature-grown GNRs@SWCNTs (c). The PL intensity redistribution takes place upon filling the SWCNTs. The PL intensity in each counter plot is normalized.

 This journal is © The Royal Society of Chemistry 2018

Published on 29 December 2017. Downloaded by Boston College on 7/14/2018 1:14:02 PM.

tubes. SWCNT PL peak position shifts upon filling have been previously reported and studied in detail for such objects as fullerenes, ferrocene, water, various organic molecules, *etc.* inside SWCNTs.[21,28,32,37] Depending on the filler the origin of the PL shifts is different. For instance, all the nanotubes demonstrate red shifts of the first optical transition after filling with water molecules.[37] Such an observation was well described within the environmental dielectric model[38] that was originally proposed for the external environment's influence on nanotube excitonic transitions. For fullerene-filled nanotubes, the origin of the shift is mainly different, especially for the narrowest filled nanotubes.[39] The opposite trend for the blue and red shifts of the E_{11} transition depending on the nanotube family type (type I (mod$(2n + m, 3) = 1$) and type II (mod$(2n + m, 3) = 2$), where n and m are nanotube indexes) clearly points out the influence of the nanotube strain. We took a closer look at the PL peak positions changes in the case of GNR filling (Fig. 3). For each nanotube geometry, the filling may result in either blue or red shifts in comparison with the values for the pristine tubes. Moreover, the changes depend on the filling temperature, proposing the different nature of the shifts for both systems. In order to see the difference between the systems we plot the shifts against the nanotube diameter and specifically point out the nanotube family type (Fig. 4). For both systems of low and high temperature polymerized GNRs inside nanotubes, we detect the blue and red shifts. The shift values are significantly smaller compared to those reported for the fullerene filling case. Nevertheless, for LT GNRs@SWCNTs the family type dependence is more prominent compared to the high temperature system. An increase of the polymerization temperature leads to more homogeneous red shifts of the PL for mostly all of the geometries, while the blue shifts get reduced. A unified expression

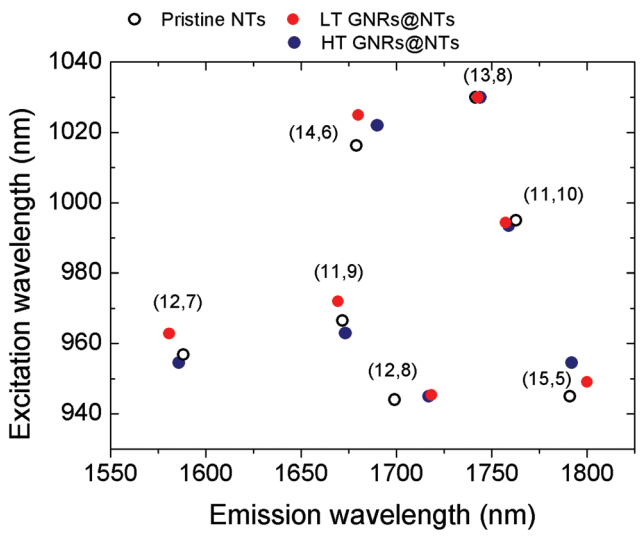

Fig. 3 PL peak position for each nanotube geometry of a pristine sample (black) and filled nanotubes with low-temperature-grown GNRs (red) and high-temperature-grown GNRs@SWCNTs (blue).

for the optical band gap modification under a small axial strain for various nanotube geometries was proposed in the work of Yang *et al.*:[40] $\Delta E = \mathrm{sign}(2p + 1)3t_0(1 + \nu)\sigma \cos 3\theta$, where σ is the axial strain, θ is the nanotube chiral angle, $\nu \approx 0.2$ is the Poisson ratio, $t_0 = 2.66$ eV is the tight-binding overlap integral, and p equals -1 or 1 for semiconducting nanotubes depending on the family type. The dependence of the sign of the band gap shift on the family type of nanotubes obtained in the experiment supports the idea that the strain after the formation of GNRs leads to the modification of nanotube optical properties in a variable degree depending on the geometry. According to the equation one percent strain can result in a maximal shift of 100 meV. In our case the strain might be up to 0.25% for (12,8) nanotubes. HR TEM imaging along with theoretical calculations[41] demonstrate a large cross-section distortion of nanotubes up to 20% of the diameter value when the graphene nanoribbons are inside,[10] which results in a local strain of the nanotube wall. According to the experimental HR TEM data some nanotubes host wide GNRs, which in principle do not fit directly to the non-disturbed tubes. The reason for the strain should lie in the polymerization procedure conditions and in the fact that initially filled molecules easily get inside during vapor phase encapsulation. Based on the PL measurements of the band gap modification upon GNR formation, we suppose that the different filling temperature results in the formation of systems with different values of perturbation. For LT GNR@SWCNT the filler nano-objects to a greater extent disturb the nanotube shape and therefore the strain effects get more prominent, while for the HT GNR@SWCNTs, the inner structures get more ordered and homogeneously fill the nanotubes, the strain effects get reduced and dielectric screening becomes more evident.

The dielectric screening effects are well pronounced for suspended SWCNTs in different external environment.[42,43] Dominantly, the excitonic energy transitions monitored *via* PL demonstrate an increase in red shifts with the increase of dielectric constant. The dependence on the environment becomes well pronounced for smaller diameter tubes with a linear trend in $(E_{11})^3\Delta E$ over d^{-5} coordinates.[43] A similar approach has been recently used for the interpretation of results of endohedral filling.[28] It should be noted that not much data is presented for the filling of large diameter nanotubes, while most of the works demonstrate the results for nanotubes with diameters around 1 nm. In our case (Fig. 5), for both types of systems a simple interpretation of the obtained results using the relationship applied for the explanation of the solvatochromic shifts in external environments with different dielectric constants becomes impossible. We detect a dependence of the optical transition on nanotube geometry and diameter. The experimental data are not well fitted by the linear function. For example, (11,9) and (12,7) species are completely out of trend for both of our systems. These geometries are also the smallest filled nanotubes; therefore the strain influence in them is expected to be maximal. The combination of several contributions should be taken into account for the interpretation of PL shifts in GNR-filled nanotubes,

Published on 29 December 2017. Downloaded by Boston College on 7/14/2018 1:14:02 PM.

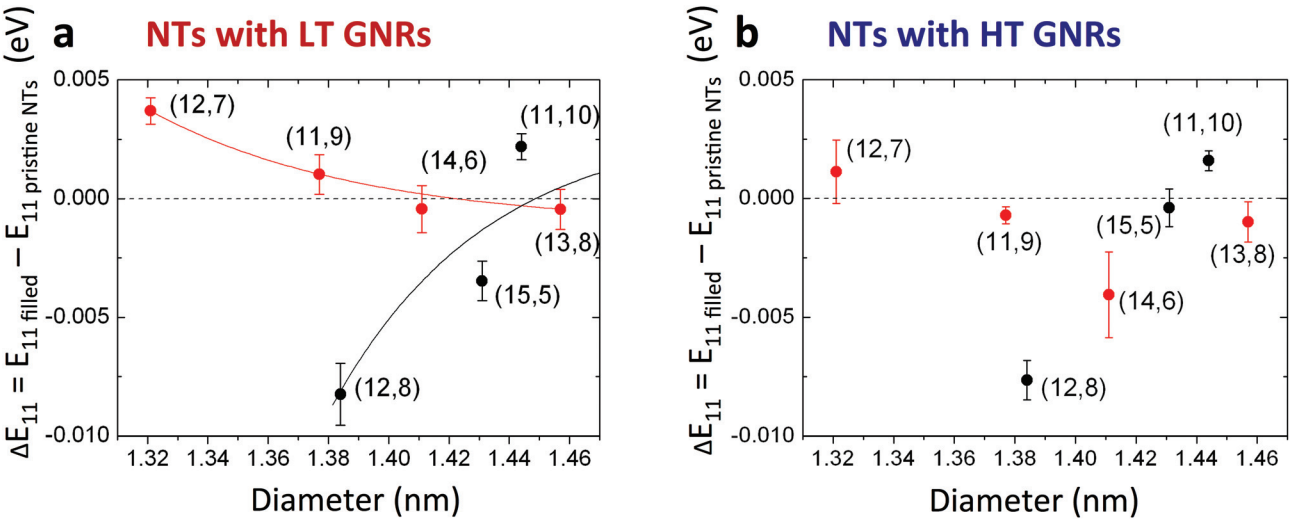

Fig. 4 The difference in the optical band gap for filled with low-temperature-grown GNRs (a) and high-temperature-grown GNRs (b) SWCNTs and pristine nanotubes plotted against nanotube diameter.

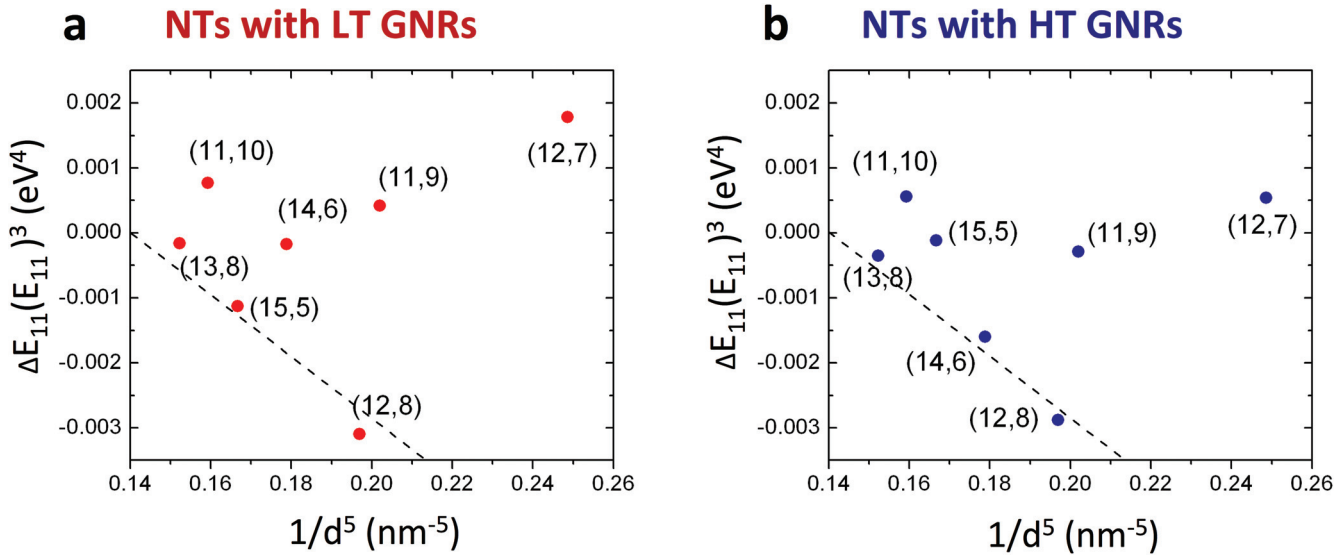

Fig. 5 Solvatochromic shift values for filled with low-temperature-grown GNRs (a) and high-temperature-grown GNRs (b) SWCNTs.

namely the dielectric screening together with the strain-induced modifications. The discrepancy from the linear trend was also reported for nanotubes filled with various molecules,[28] which might be explained not only by the strain, but also by the specific molecule organizations depending on the nanotube diameter.[33]

We now turn to a discussion of PL intensity redistribution between the nanotube geometries upon filling. The gradual change in the nanotube PL intensity in both systems of high- and low-temperature polymerized GNRs inside SWCNTs is clearly seen in Fig. 2. For the pristine sample the dominant emitting tubes possess the smallest diameters in the ensemble. After the formation of GNRs inside at low temperature, (14,6) geometry becomes the brightest. For the GNRs polymerized at high temperature the emphasis shifts towards the (13,8) geometry. The change in the PL emission properties of nanotubes is governed by the inner structures. Encapsulation of different fillers may result in both an increase and also quenching of nanotube PL. Frequently, the main origin of the phenomena is an electron transfer between the core and the shell.[25,27] In the case of suspended and filled nanotubes additional factors may come into play, such as oxidation during the opening procedure and interaction with surfactant molecules.[27] Moreover, a complicated interplay between the inner structure charge transfer and the intrinsic charge transfer from the outer tube influenced by the external environment can also take place.[30] In our two types of systems we used the same procedures for the preparation of nanotubes and identi-

 This journal is © The Royal Society of Chemistry 2018

Published on 29 December 2017. Downloaded by Boston College on 7/14/2018 1:14:02 PM.

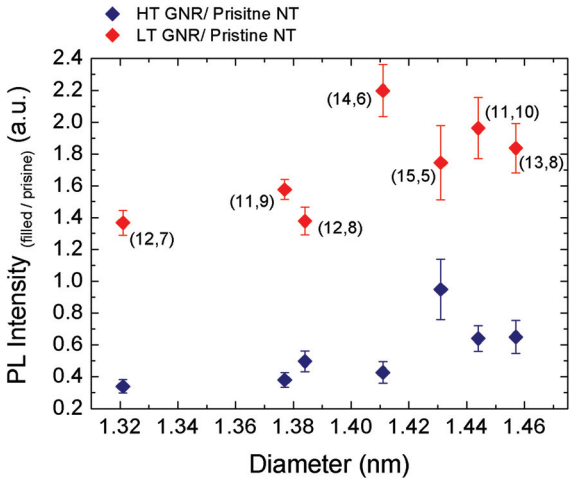

Fig. 6 PL intensity ratio between filled (with low temperature polymerized GNRs – red color, high temperature – blue color) and pristine SWCNTs as a function of tube diameter. Note the specific nanotube geometries demonstrating the PL increase upon filling, (14,6) for red and (15,5) for blue points. For both systems there is a slight PL increase trend for larger nanotube diameters.

cal surfactant concentrations in order to detect and compare the changes assigned to the influence of the inner structure. We plot the PL intensity against nanotube diameter after filling compared to pristine nanotubes for each geometry (Fig. 6). The common trend for both systems is the PL intensity increase for the larger diameter tubes. This can be attributed to the exciton energy transfer to the nanotubes with the narrower band gaps.[44] However, a new detected feature is the PL increase for the nanotubes that don't possess the narrowest band gaps in the sample. For nanotubes filled with low temperature GNRs the (14,6) geometry demonstrates the highest PL increase, while for the tubes with GNRs grown at high temperature the emission maximum is shifted towards the larger diameter species. The organization of the inner structures inside the tube should be the main reason for the PL intensity redistribution between nanotubes with various geometries. As demonstrated previously for ferrocene molecules[33] a specific orientation of encapsulated structures results in different intermolecular interactions, which may lead to an increase of the PL intensity. In the case of GNRs@SWCNTs a specific relationship between the nanotube diameter and the inner structure configuration can be explained by the promoted intermolecular interaction between the filler molecules during the polymerization that results in the unique orientation of the formed GNR within the tube. At high temperature GNRs fill the nanotube channel more homogeneously; the inner structure is well organized and the modification to the nanotube environment is uniform. With the exception of the optimal nanotube geometries, a large number of small diameter nanotubes demonstrate a quenched PL. The whole guest–host system becomes a unified structure, similar to the DWCNTs, where the charge transfer from the outer shell to the inner tube is presented for all of the geometries.[45] The behavior of the stepwise PL intensity redistribution between the nanotube geometries was observed in the case of PTCDA molecules filling inside laser ablation SWCNTs and their further transformation into GNRs in the inner nanotube space at 500 °C.[6,private communication]

The PL quantum yields of the two types of filled nanotubes with low and high temperature polymerized GNRs are significantly different (Fig. 7). For SWCNTs with the low temperature GNRs inside, we detect the intensity gain of ≈1.7 compared to the pristine tubes, while for the SWCNTs with the high temperature GNRs, conversely, we detect an intensity reduction. Whereas for the high temperature system the decrease in intensity can be explained by a charge transfer from the shell to the uniformly organized long GNR inside, the increase of the quantum yield for the low temperature system might have several explanations. We are able to exclude the influence of the bundling between the tubes as the surfactant concentrations and other preparation procedures for both samples are the same. In order to increase the overall PL quantum yield for all of the nanotube geometries the non-radiative relaxation rate of excitons should be reduced, *i.e.* the interaction of excitons with the quenching sites. Previously, we had estimated that the difference between two systems lies in the organization of the inner structures inside nanotubes. The larger induced strain in SWCNTs (taking place in the case of the low temperature GNRs inside the NT system) itself is not responsible for the quantum yield change.[46,47] However, a repeatable bending of the tube, as in the case when the inner structures can be short and not completely polymerized, may lead to a localization of the excitons that are responsible for the brightening.[48] The peculiar local charge transfer for the more perturbed system of not fully polymerized GNRs can be con-

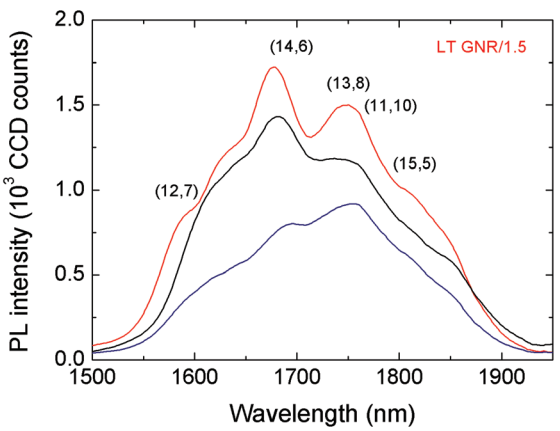

Fig. 7 PL spectra from a pristine sample (black) and filled nanotubes with the low temperature GNRs (red) and high temperature GNRs@SWCNTs (blue). An excitation was performed at 1022 nm wavelength. The original response from SWCNTs filled with the low temperature polymerized GNRs was divided by 1.5. The spectra are normalized according to optical density.

Published on 29 December 2017. Downloaded by Boston College on 7/14/2018 1:14:02 PM.

sidered as another explanation. Similarly to the case of linear carbon chains inside double-walled carbon nanotubes,[30] charge transfer between the encapsulated structures, which according to the C_s-HRTEM image simulation[5] might contain two sets of ribbons inside, can exist not only from the shell to the ribbon, but also between the inner structures modulating the overall result.

For both types of nanotube–GNR systems the PL measurements in a wider excitation range don't allow detection of the energy transfer from the ribbons to the nanotubes, *i.e.* with the excitation of GNRs in the UV-vis spectral region and detection of nanotube response in the near-IR range. That means that there is no strong interaction between the nanotube and the filler. In Raman measurements the G band peak positions are not shifted upon filling, which signs a weak charge transfer ESI Fig. S1, S2,† and ref. 5, 21. The Raman measurements give information on several geometries of the nanotubes in the ensemble satisfying the "in"- and "out"-going resonance conditions on the exact wavelength. Similar to optical absorbance spectroscopy, monitoring the G band peak position in the Raman measurements usually doesn't allow a complete disentangling of the response from each nanotube geometry in our experiment. However, the charge transfer can still be the origin of the PL quantum yield increase as it may specifically be present for only limited nanotube species satisfying certain conditions such as the exact diameter value. PL measurements allowed us to detect the peculiar effects of certain nanotube geometries upon filling. The precise modification of the nanotube optical band gap, together with the change of PL quantum yield, was detected for a limited number of geometries and is defined by the inner structure organization.

Conclusions

We demonstrated the influence of filled hydrogenated graphene nanoribbons on the optical properties of host SWCNTs. We compare two nanoscale systems, one with low- and another with high-temperature polymerized GNRs inside nanotubes. The band gap modification of the host semiconducting nanotubes is accessed *via* photoluminescence excitation mapping. The interplay of strain and dielectric screening affects the PL shifts for both types of systems to varying degrees. We detect the stepwise PL intensity redistribution between the nanotube geometries upon the increase of the polymerization temperature of the inner GNRs. The enhancement of PL quantum yield of specific nanotube diameters upon filling was assigned to the optimal organization of the inner structures. Our findings demonstrate the existence of an exact match between the nanotube geometry and the inner structure resulting in the peculiar optical properties. Owing to the recent progress in separation techniques of nanotubes with a single geometry type, tailoring and precise modification of electronic and optical properties upon filling in order to enhance the effects for exact applications becomes feasible.

Conflicts of interest

There are no conflicts to declare.

Acknowledgements

This work was supported by the RSF 15-12-30041. We acknowledge the fruitful discussion with Dr. Dmitry Rybkovskiy. A. I. C. acknowledges support from the Alexander von Humboldt Foundation. Z. L. and K. S. acknowledge support from a Grant-in-Aid for Scientific Research on Innovative Areas (MEXT KAKENHI Grant Number 25107003).

References

1 T. W. Chamberlain, J. Biskupek, S. T. Skowron, A. V. Markevich, S. Kurasch, O. Reimer, K. E. Walker, G. A. Rance, X. Feng, K. Müllen, A. Turchanin, M. A. Lebedeva, A. G. Majouga, V. G. Nenajdenko, U. Kaiser, E. Besley and A. N. Khlobystov, *ACS Nano*, 2017, **11**, 2509–2520.
2 S. Cambré, J. Campo, C. Beirnaert, C. Verlackt, P. Cool and W. Wenseleers, *Nat. Nanotechnol.*, 2015, **10**, 248–252.
3 E. Gaufrès, N. Y. W. Tang, A. Favron, C. Allard, F. Lapointe, V. Jourdain, S. Tahir, C. N. Brosseau, R. Leonelli and R. Martel, *ACS Nano*, 2016, **10**, 10220–10226.
4 M. Tange, T. Okazaki, Z. Liu, K. Suenaga and S. Iijima, *Nanoscale*, 2016, **8**, 7834–7839.
5 H. E. Lim, Y. Miyata, M. Fujihara, S. Okada, Z. Liu, Arifin, K. Sato, H. Omachi, R. Kitaura, S. Irle, K. Suenaga and H. Shinohara, *ACS Nano*, 2015, **9**, 5034–5040.
6 H. E. Lim, Y. Miyata, R. Kitaura, Y. Nishimura, Y. Nishimoto, S. Irle, J. H. Warner, H. Kataura and H. Shinohara, *Nat. Commun.*, 2013, **4**, 2548.
7 A. V. Talyzin, I. V. Anoshkin, A. V. Krasheninnikov, R. M. Nieminen, A. G. Nasibulin, H. Jiang and E. I. Kauppinen, *Nano Lett.*, 2011, **11**, 4352–4356.
8 B. W. Smith, M. Monthioux and D. E. Luzzi, *Nature*, 1998, **396**, 323–324.
9 A. S. Sinitsa, T. W. Chamberlain, T. Zoberbier, I. V. Lebedeva, A. M. Popov, A. A. Knizhnik, R. L. McSweeney, J. Biskupek, U. Kaiser and A. N. Khlobystov, *Nano Lett.*, 2017, **17**, 1082–1089.
10 A. Chuvilin, E. Bichoutskaia, M. C. Gimenez-Lopez, T. W. Chamberlain, G. A. Rance, N. Kuganathan, J. Biskupek, U. Kaiser and A. N. Khlobystov, *Nat. Mater.*, 2011, **10**, 687–692.
11 S. A. Miners, G. A. Rance and A. N. Khlobystov, *Chem. Soc. Rev.*, 2016, **45**, 4727–4746.
12 H.-P. Komsa, R. Senga, K. Suenaga and A. V. Krasheninnikov, *Nano Lett.*, 2017, **17**, 3694–3700.
13 M. Hart, E. R. White, J. Chen, C. M. McGilvery, C. J. Pickard, A. Michaelides, A. Sella, M. S. P. Shaffer and

 This journal is © The Royal Society of Chemistry 2018

Published on 29 December 2017. Downloaded by Boston College on 7/14/2018 1:14:02 PM.

C. G. Salzmann, *Angew. Chem., Int. Ed.*, 2017, **56**, 8144–8148.
14 A. A. Eliseev, N. S. Falaleev, N. I. Verbitskiy, A. A. Volykhov, L. V. Yashina, A. S. Kumskov, V. G. Zhigalina, A. L. Vasiliev, A. V. Lukashin, J. Sloan and N. A. Kiselev, *Nano Lett.*, 2017, **17**, 805–810.
15 A. A. Tonkikh, D. V. Rybkovskiy, A. S. Orekhov, A. I. Chernov, A. A. Khomich, C. P. Ewels, E. I. Kauppinen, S. B. Rochal, A. L. Chuvilin and E. D. Obraztsova, *Carbon*, 2016, **109**, 87–97.
16 L. Shi, P. Rohringer, K. Suenaga, Y. Niimi, J. Kotakoski, J. C. Meyer, H. Peterlik, M. Wanko, S. Cahangirov, A. Rubio, Z. J. Lapin, L. Novotny, P. Ayala and T. Pichler, *Nat. Mater.*, 2016, **15**, 634–639.
17 T. Okazaki, Y. Iizumi, S. Okubo, H. Kataura, Z. Liu, K. Suenaga, Y. Tahara, M. Yudasaka, S. Okada and S. Iijima, *Angew. Chem., Int. Ed.*, 2011, **50**, 4853–4857.
18 I. V. Anoshkin, A. V. Talyzin, A. G. Nasibulin, A. V. Krasheninnikov, H. Jiang, R. M. Nieminen and E. I. Kauppinen, *ChemPhysChem*, 2014, **15**, 1660–1665.
19 A. I. Chernov, P. V. Fedotov, I. V. Anoshkin, A. G. Nasibulin, E. I. Kauppinen, V. L. Kuznetsov and E. D. Obraztsova, *Phys. Status Solidi B*, 2014, **251**, 2372–2377.
20 M. Fujihara, Y. Miyata, R. Kitaura, Y. Nishimura, C. Camacho, S. Irle, Y. Iizumi, T. Okazaki and H. Shinohara, *J. Phys. Chem. C*, 2012, **116**, 15141–15145.
21 A. I. Chernov, P. V. Fedotov, A. V. Talyzin, I. S. Lopez, I. V. Anoshkin, A. G. Nasibulin, E. I. Kauppinen and E. D. Obraztsova, *ACS Nano*, 2013, 6346–6353.
22 X. Wei, T. Tanaka, Y. Yomogida, N. Sato, R. Saito and H. Kataura, *Nat. Commun.*, 2016, **7**, 12899.
23 V. A. Eremina, P. A. Obraztsov, P. V. Fedotov, A. I. Chernov and E. D. Obraztsova, *Phys. Status Solidi*, 2017, **254**, 1600659.
24 A. I. Chernov, V. A. Eremina, J. Shook, A. Collins, P. Walker, P. V. Fedotov, A. A. Zakhidov and E. D. Obraztsova, *Phys. Status Solidi*, 2018, 1700139.
25 T. Takenobu, T. Takano, M. Shiraishi, Y. Murakami, M. Ata, H. Kataura, Y. Achiba and Y. Iwasa, *Nat. Mater.*, 2003, **2**, 683–688.
26 M. Sauer, H. Shiozawa, P. Ayala, G. Ruiz-Soria, X. Liu, A. Chernov, S. Krause, K. Yanagi, H. Kataura and T. Pichler, *Carbon*, 2013, **59**, 237–245.
27 X. Liu, H. Kuzmany, P. Ayala, M. Calvaresi, F. Zerbetto and T. Pichler, *Adv. Funct. Mater.*, 2012, **22**, 3202–3208.
28 J. Campo, Y. Piao, S. Lam, C. M. Stafford, J. K. Streit, J. R. Simpson, A. R. Hight Walker and J. A. Fagan, *Nanoscale Horiz.*, 2016, **1**, 317–324.
29 X. Ma, S. Cambré, W. Wenseleers, S. K. Doorn and H. Htoon, *Phys. Rev. Lett.*, 2017, **118**, 27402.
30 P. Rohringer, L. Shi, P. Ayala and T. Pichler, *Adv. Funct. Mater.*, 2016, **26**, 4874–4881.
31 J. Lee, H. Kim, S.-J. Kahng, G. Kim, Y.-W. Son, J. Ihm, H. Kato, Z. W. Wang, T. Okazaki, H. Shinohara and Y. Kuk, *Nature*, 2002, **415**, 1005–1008.
32 T. Okazaki, S. Okubo, T. Nakanishi, S.-K. Joung, T. Saito, M. Otani, S. Okada, S. Bandow and S. Iijima, *J. Am. Chem. Soc.*, 2008, **130**, 4122–4128.
33 Y. Iizumi, H. Suzuki, M. Tange and T. Okazaki, *Nanoscale*, 2014, **6**, 13910–13914.
34 A. V. Talyzin, I. V. Anoshkin and A. G. Nasibulin, *Phys. Status Solidi*, 2015, **252**, 2491–2495.
35 J.-D. R. Rocha, S. M. Bachilo, S. Ghosh, S. Arepalli and R. B. Weisman, *Anal. Chem.*, 2011, **83**, 7431–7437.
36 T. W. Chamberlain, J. Biskupek, S. T. Skowron, P. A. Bayliss, E. Bichoutskaia, U. Kaiser and A. N. Khlobystov, *Small*, 2015, **11**, 622–629.
37 S. Cambré, S. M. Santos, W. Wenseleers, A. R. T. Nugraha, R. Saito, L. Cognet and B. Lounis, *ACS Nano*, 2012, **6**, 2649–2655.
38 A. R. T. Nugraha, R. Saito, K. Sato, P. T. Araujo, A. Jorio and M. S. Dresselhaus, *Appl. Phys. Lett.*, 2010, **97**, 91905.
39 S. Okubo, T. Okazaki, N. Kishi, S. K. Joung, T. Nakanishi, S. Okada and S. Iijima, *J. Phys. Chem. C*, 2009, **113**, 571–575.
40 L. Yang and J. Han, *Phys. Rev. Lett.*, 2000, **85**, 154–157.
41 A. V. Osadchy, I. V. Vorobyev, D. V. Rybkovskiy and E. D. Obraztsova, *J. Nanoelectron. Optoelectron.*, 2013, **8**, 91–94.
42 Y. Ohno, S. Iwasaki, Y. Murakami, S. Kishimoto, S. Maruyama and T. Mizutani, *Phys. Status Solidi B*, 2007, **244**, 4002–4005.
43 C. A. Silvera-Batista, R. K. Wang, P. Weinberg and K. J. Ziegler, *Phys. Chem. Chem. Phys.*, 2010, **12**, 6990.
44 P. H. Tan, A. G. Rozhin, T. Hasan, P. Hu, V. Scardaci, W. I. Milne and A. C. Ferrari, *Phys. Rev. Lett.*, 2007, **99**, 137402.
45 V. Zólyomi, J. Koltai, Á. Rusznyák, J. Kürti, Á. Gali, F. Simon, H. Kuzmany, Á. Szabados and P. R. Surján, *Phys. Rev. B: Condens. Matter Mater. Phys.*, 2008, **77**, 245403.
46 O. Kiowski, S. S. Jester, S. Lebedkin, Z. Jin, Y. Li and M. M. Kappes, *Phys. Rev. B: Condens. Matter Mater. Phys.*, 2009, **80**, 75426.
47 C. D. Spataru and F. Léonard, *Phys. Rev. B: Condens. Matter Mater. Phys.*, 2013, **88**, 45404.
48 C. Georgi, A. A. Green, M. C. Hersam and A. Hartschuh, *ACS Nano*, 2010, **4**, 5914–5920.